Optimized topological quantum compilation of three-qubit controlled gates in the Fibonacci anyon model: A controlled-injection approach

Abdellah Tounsi [1,2] Nacer Eddine Belaloui [1,2] Mohamed Messaoud Louamri [1,3]
Achour Benslama [1,2] and Mohamed Taha Rouabah [1,2,*]

[1]*Constantine Quantum Technologies, University Constantine 1 Frères Mentouri, Ain El Bey Road, Constantine 25017, Algeria*
[2]*Laboratoire de Physique Mathématique et Subatomique, University Constantine 1 Frères Mentouri, Ain El Bey Road, Constantine 25017, Algeria*
[3]*Theoretical Physics Laboratory, University of Science and Technology Houari Boumediene, BP 32 Bab Ezzouar, Algiers 16111, Algeria*

(Received 3 January 2024; revised 25 April 2024; accepted 22 May 2024; published 1 July 2024)

A method, termed controlled injection, is proposed for compiling three-qubit controlled gates within the non-Abelian Fibonacci anyon model. Building on single-qubit compilation techniques with three Fibonacci anyons, the approach showcases enhanced accuracy and reduced braid length compared to the conventional decomposition method for the controlled three-qubit gates. This method necessitates only four two-qubit gates for decomposition, a notable reduction from the conventional five. In conjunction, the study introduces a class of controlled three-qubit gates and conducts a numerical simulation of the topological *i*Toffoli gate to validate the approach. In addition, we propose an optimization method for single-qubit gate approximation using algebraic relations and numerical methods, including distributed computing.

DOI: 10.1103/PhysRevA.110.012603

I. INTRODUCTION

In the previous two decades, there has been a significant interest in topological quantum computation (TQC) due to its potential for scalable and fault-tolerant quantum computing. The latter is crucial for fully harnessing the capabilities of quantum systems [1–7]. The foundation of TQC relies on the existence of anyons, which were proposed by Leinaas and Myrheim in 1976 [8] and quantum mechanically formulated by Wilczek in 1982 [9]. In (2+1) space-time dimensions, particles can exhibit anyonic statistics, in contrast to the (3+1) dimensions where particles are either bosons or fermions. Consequently, the quantum evolution of anyons moving around each other in an effective two-dimensional space is determined by a topological phase that is independent of the system's dynamics and geometry in the same spirit of the Aharonov-Bohm phase of an electron moving around a confined magnetic flux [9]. Additionally, within the framework of topological quantum field theory (TQFT), anyon models can be described using braided monoidal category theories [10]. In this context, there exists a correspondence between the topological invariants of knots and the quantum observables of the anyonic system [11]. In theory, a class of anyons can be described within the Chern-Simons quantum field theory. This theory is celebrated because of its successful description of the fractional quantum Hall effect (FQHE) [12]. Specifically, the SU(2) non-Abelian version of this theory produces the $SU(2)_k$ anyon models, which include the most famous Ising and Fibonacci (Yang-Lee) models for $k = 2$ and $k = 3$, respectively. It is proven that $SU(2)_k$ anyon models are Turing complete for $k = 3$ and $k \geqslant 5$ [13,14], while the $SU(2)_2$ model covers only the Clifford group. On the other hand, anyons can emerge in some types of topological lattice models. In his seminal work, Kitaev proposed the toric code and quantum doubles as quantum error correction codes that possess topological ground states protected by an energy gap [2]. In this framework, Abelian and non-Abelian anyons emerge as excitations and serve as quantum information processing agents. Recently, a modified version of the surface code has been simulated in a superconducting quantum processor, providing evidence of the non-Abelian statistics of Ising anyons [15]. At the same time, a quantum double code based on the dihedral group D_4 implemented on a trapped-ion quantum processor demonstrated experimental observation of non-Abelian anyon statistics [16]. Moreover, the experimental results from various condensed matter systems provide compelling evidence in support of the realization of topological quantum computing systems in the near future. Specifically, it has been shown experimentally that the quasiparticles in the fractional quantum Hall systems exhibit anyonic statistics [17,18]. Furthermore, a recent study suggests the possibility of detecting Majorana zero modes in semiconductor-superconductor heterostructure devices [19].

However, the compilation of quantum circuits in the TQC framework is not generally trivial. Although the Fibonacci anyon model ensures universality and is dense in the special unitary group, significant efforts have been devoted to achieving an efficient and optimal compilation scheme. Numerous algorithms are available to map SU(2) quantum gates to topological braiding operations within Fibonacci anyons,

*Contact author: m.taha.rouabah@umc.edu.dz

including the Solovay-Kitaev algorithm [20], the brute-force algorithm [7,21], the evolutionary algorithm [22], and deep reinforcement learning [23]. Additionally, an asymptotically optimal and systematic algorithm based on ring theory has been specifically designed for certain SU(2) quantum gates with Fibonacci anyons [24]. Moreover, a recently developed generic Monte Carlo approach has been introduced to compile near-optimal braid words at the single-qubit level in $SU(2)_k$ anyon models [25].

Additionally, it is necessary to compile two-qubit gates, such as the controlled-NOT (CNOT) gate, to ensure universality. In this context, several procedures have been proposed. Specifically, an injection method was introduced by Bonesteel *et al.* [26] to compose two-qubit gates from single-qubit gates of Fibonacci anyons. Another iterative procedure has been designed to systematically generate entangling two-qubit Fibonacci anyon braids [27]. Even though the compilation of any single-qubit gate along with the CNOT gate is sufficient to demonstrate the quantum computing universality of a given anyon model, the implementation of larger quantum circuits may require reduced compilation schemes to decrease processing time. Specifically, the Toffoli gate, or the CNOT gate, can be decomposed by concatenation of five two-qubit controlled gates [28]. However, the pertinent query revolves around the feasibility of reducing this requisite. In this context, a general compilation scheme based on dense encoding was proposed to construct the controlled-controlled phase gate for a wide range of anyon models using six successive gates acting on three qubits densely encoded on eight anyons [29]. This method does not address a wide range of controlled-controlled gates such as the CNOT and Deutsch gates. In this study, we present a procedure that we call controlled injection to construct a class of controlled three-qubit gates within the Fibonacci anyon model. The controlled-injection method offers the advantage of reducing the complexity of the braids compared to the conventional decomposition method. We demonstrate our finding by comparing the resulting *i*Toffoli gates using both approaches. To ensure an accurate comparison using the most optimal compilation possible, we employ the brute-force algorithm and implement several optimizations based on algebraic and numerical techniques, given the computational complexity of the brute-force algorithm. Furthermore, the controlled-injection method introduces unusual quantum logic gates that can be used in specific applications.

This paper begins by introducing the fundamentals of quantum computing with Fibonacci anyons, along with essential notations. We then delve into the key aspects of compiling single-qubit gates within the Fibonacci model, using the brute-force algorithm. Thereafter, we present the controlled injection method, supplemented by a class of controlled three-qubit gates. We conclude our study with a comparative analysis between our method and the conventional decomposition approach.

II. FIBONACCI MODEL

The Fibonacci anyon model is the simplest universal anyon model among the $SU(2)_k$ family. Fibonacci anyons can theoretically emerge as quasiparticles in the FQHE at 12/5 filling factor [30]. They can also appear as defects in the so-called string-net (Levin-Wen) lattice models [31,32]. In the Fibonacci model, we have only one nontrivial anyonic charge, referred to as **1**, along with the trivial vacuum charge, **0**. The nontrivial Fibonacci fusion rule is defined as follows [21,33,34]:

$$\mathbf{1} \times \mathbf{1} = \mathbf{0} + \mathbf{1}. \tag{1}$$

The dimension of the fusion space $\mathcal{F}$ in terms of the number of Fibonacci anyons follows the famous Fibonacci series such that $\dim(\mathcal{F}_{n+2}) = \dim(\mathcal{F}_n) + \dim(\mathcal{F}_{n+1})$, where n is the number of anyons, as shown in Table I. Notice that a qubit can be represented minimally by three or four anyons. While two anyons introduce a trivial braid operation, three anyons form a qubit with overall charge **1** and correspond to the minimum qubit representation with Fibonacci anyons. Namely, all possible fusion processes for three Fibonacci anyons associated with logical states are

$$|0\rangle = |\mathbf{0}, \mathbf{1}\rangle = |((\mathbf{1}, \mathbf{1})_{\mathbf{0}}, \mathbf{1})_{\mathbf{1}}\rangle, \tag{2}$$

$$|1\rangle = |\mathbf{1}, \mathbf{1}\rangle = |((\mathbf{1}, \mathbf{1})_{\mathbf{1}}, \mathbf{1})_{\mathbf{1}}\rangle, \tag{3}$$

$$|2\rangle = |\mathbf{1}, \mathbf{0}\rangle = |((\mathbf{1}, \mathbf{1})_{\mathbf{1}}, \mathbf{1})_{\mathbf{0}}\rangle, \tag{4}$$

such that $|i, j\rangle$ refers to the fusion state $|((\mathbf{1}, \mathbf{1})_i, \mathbf{1})_j\rangle$ for reduction. The sector of an overall charge **0** is trivial with a singular state $\{|0\rangle\}$. Four anyons with an overall charge **0** also form a qubit. Namely, four Fibonacci anyons allow the following fusion states:

$$|0\rangle = |\mathbf{0}, \mathbf{1}, \mathbf{0}\rangle = |(((\mathbf{1}, \mathbf{1})_{\mathbf{0}}, \mathbf{1})_{\mathbf{1}}, \mathbf{1})_{\mathbf{0}}\rangle, \tag{5}$$

$$|1\rangle = |\mathbf{1}, \mathbf{1}, \mathbf{0}\rangle = |(((\mathbf{1}, \mathbf{1})_{\mathbf{1}}, \mathbf{1})_{\mathbf{1}}, \mathbf{1})_{\mathbf{0}}\rangle, \tag{6}$$

$$|2\rangle = |\mathbf{1}, \mathbf{0}, \mathbf{1}\rangle = |(((\mathbf{1}, \mathbf{1})_{\mathbf{1}}, \mathbf{1})_{\mathbf{0}}, \mathbf{1})_{\mathbf{1}}\rangle, \tag{7}$$

$$|3\rangle = |\mathbf{0}, \mathbf{1}, \mathbf{1}\rangle = |(((\mathbf{1}, \mathbf{1})_{\mathbf{0}}, \mathbf{1})_{\mathbf{1}}, \mathbf{1})_{\mathbf{1}}\rangle, \tag{8}$$

$$|4\rangle = |\mathbf{1}, \mathbf{1}, \mathbf{1}\rangle = |(((\mathbf{1}, \mathbf{1})_{\mathbf{1}}, \mathbf{1})_{\mathbf{1}}, \mathbf{1})_{\mathbf{1}}\rangle. \tag{9}$$

While the sector **0** forms a qubit, the sector **1** forms a qutrit as we are going to see later. Representing a qubit with more than four anyons is not recommended since it provokes leakage, as proven for all anyon models [35].

To compute the matrix representation of the braid generators of a given set of anyons, the fusion matrix F that defines

TABLE I. Size of the fusion space $\mathcal{F}_n$ in function of the number of anyons n. $\dim(\mathcal{F}_n^{\mathbf{0}})$ is the dimension of the fusion space given that the total charge is **0**, while $\dim(\mathcal{F}_n^{\mathbf{1}})$ is the size of the fusion space given that the overall charge is **1**. Finally, $\dim(\mathcal{F}_n)$ is the total size of the fusion space.

n	$\dim\left(\mathcal{F}_n^{\mathbf{0}}\right)$	$\dim\left(\mathcal{F}_n^{\mathbf{1}}\right)$	$\dim(\mathcal{F}_n)$
1	0	1	1
2	1	1	2
3	1	2	3
4	2	3	5
n	$\sum_{i=1,2}\dim\left(\mathcal{F}_{n-i}^{\mathbf{0}}\right)$	$\sum_{i=1,2}\dim\left(\mathcal{F}_{n-i}^{\mathbf{1}}\right)$	$\sum_{i=1,2}\dim(\mathcal{F}_{n-i})$

the basis transformation,

$$|((a,b)_i,c)_j\rangle = \sum_k \left(F^j_{abc}\right)_{ik} |(a,(b,c)_k)_j\rangle, \tag{10}$$

and the rotation matrix R_{ab} that defines the operation of exchanging two anyons a and b with a specific fusion outcome,

$$R_{ab}|(a,b)_i\rangle = R^i_{ab}|(b,a)_i\rangle, \tag{11}$$

are required. Solving the pentagon identities reveals one nontrivial fusion matrix F^1_{111} for the Fibonacci model given by [4,33]

$$F^{\mathbf{1}}_{\mathbf{111}} = \begin{pmatrix} \left(F^{\mathbf{1}}_{\mathbf{111}}\right)^{\mathbf{0}}_{\mathbf{0}} & \left(F^{\mathbf{1}}_{\mathbf{111}}\right)^{\mathbf{0}}_{\mathbf{1}} \\ \left(F^{\mathbf{1}}_{\mathbf{111}}\right)^{\mathbf{1}}_{\mathbf{0}} & \left(F^{\mathbf{1}}_{\mathbf{111}}\right)^{\mathbf{1}}_{\mathbf{1}} \end{pmatrix} = \begin{pmatrix} \tau & \sqrt{\tau} \\ \sqrt{\tau} & -\tau \end{pmatrix}, \tag{12}$$

up to a global phase, where τ is the inverse of the golden ratio. Then, solving the hexagon identities gives the right-handed and the left-handed solutions of the rotation matrix $R_{\mathbf{11}}$ [4,33]:

$$R_{\mathbf{11}} = \begin{pmatrix} R^{\mathbf{0}}_{\mathbf{11}} & R^{\mathbf{01}}_{\mathbf{11}} \\ R^{\mathbf{10}}_{\mathbf{11}} & R^{\mathbf{1}}_{\mathbf{11}} \end{pmatrix} = \begin{pmatrix} e^{\pm i4\pi/5} & 0 \\ 0 & -e^{\pm i2\pi/5} \end{pmatrix}, \tag{13}$$

up to a global phase. Here, the $(+)$ and $(-)$ signs in the exponents refer to right-handed and left-handed twisting, respectively. The off-diagonal components of $R_{\mathbf{11}}$ are null because exchanging two particles preserves the fusion outcome.

Braiding, a fundamental operation in anyon models, consists of exchanging two adjacent anyons. The braiding operation between the nth and $(n+1)$th particles is denoted by the σ_n braid operator. In this work, all the necessary braid operators matrix representations are calculated using a systematic numerical method developed in [36]. It is sufficient to play with F and R transformations to express all braiding operations. The main ingredient of this procedure is the braiding matrix B that defines the exchange of any two adjacent anyons b and c as follows:

$$B_{bc}|((a,b)_i,c)_j\rangle = \sum_k \left(B^j_{abc}\right)^i_k |((a,c)_k,b)_j\rangle, \tag{14}$$

such that $B^j_{abc} = F^j_{abc} R_{bc} F^{\dagger j}_{acb}$. This formula is generic whenever the fusion state is in the form $|(\cdots((a_0,a_1)_{i_1},a_2)_{i_2},\cdots a_n)_{i_n}\rangle$. Consequently, in the case of three Fibonacci anyons, we find that the braid operations' matrix components that describe the transitions between the basis states in Eqs. (4), (2), and (3) are given as follows:

$$\langle i',j'|\sigma_1|i,j\rangle = R^i_{\mathbf{11}}\delta_{ii'}\delta_{jj'}, \tag{15}$$

$$\langle i',j'|\sigma_2|i,j\rangle = \left(B^j_{\mathbf{111}}\right)^i_{i'}\delta_{jj'}. \tag{16}$$

Similarily, we can conclude the matrix representation of σ_1, σ_2, and σ_3 acting on four Fibonacci anyons in the basis states Eqs. (5), (6), (7), and (8):

$$\langle i',j',k'|\sigma_1|i,j,k\rangle = R^i_{\mathbf{11}}\delta_{ii'}\delta_{jj'}\delta_{kk'}, \tag{17}$$

$$\langle i',j',k'|\sigma_2|i,j,k\rangle = \sum_m \left(B^j_{\mathbf{111}}\right)^i_m \delta_{mi'}\delta_{jj'}\delta_{kk'}, \tag{18}$$

$$\langle i',j',k'|\sigma_3|i,j,k\rangle = \sum_m \left(B^k_{i\mathbf{11}}\right)^j_m \delta_{ii'}\delta_{mj'}\delta_{kk'}, \tag{19}$$

such that

$$B^{\mathbf{1}}_{\mathbf{111}} = \begin{pmatrix} e^{-i6\pi/5}\tau & e^{-i3\pi/5}\sqrt{\tau} \\ e^{-i3\pi/5}\sqrt{\tau} & -\tau \end{pmatrix} \tag{20}$$

up to a global phase, while other B components are trivial.

Before going further on the quantum computing with single and multiple qubits using the Fibonacci model, it is worthy to note that the dimension of the fusion space of anyons differs from that of the Hilbert space of qubits. For instance, simulating two qubits requires a fusion space of size four or larger. In the context of Fibonacci models, two practical options arise. The first is to use five anyons prepared with an overall charge of **1**, resulting in a fusion space of five dimensions. The second is to allocate three anyons to each qubit, resulting in five and eight fusion states depending on whether the overall charge is **0** or **1**, respectively. The former option, termed dense encoding, is considered optimal in terms of resource utilization. The latter, called sparse encoding, is compatible with the picture of quantum circuits decomposed into separate qubits. A general scheme for gate compilation within the dense encoding framework is explored in [29]. However, in this work, we opt for sparse encoding, aligning with the mainstream [7,26,37]. Additionally, this study demonstrates several advantages of this convention.

III. COMPILING SINGLE-QUBIT GATES

The algebraic group generated by Fibonacci braiding operations is densely mapped to the SU(N) group and is polynomially equivalent to a quantum circuit [13,14]. In the context of three Fibonacci anyons, the matrix representation $\rho(\Sigma)$ of any Fibonacci braid sequence Σ of σ_1 and σ_2 given in Eqs. (15) and (16) assumes a general form [37],

$$\rho(\Sigma) = \left(\begin{array}{c|c} \pm e^{-iW(\Sigma)\pi/10}[\mathrm{SU}(2)] & \\ \hline & e^{i3W(\Sigma)\pi/5} \end{array}\right), \tag{21}$$

acting on the basis states Eqs. (4), (2), and (3), where $W(\Sigma)$, the winding number, is defined as the sum of the powers of the braid sequence. Consequently, the global phase of Σ in both blocks is determined solely by the winding number, up to a $\pm$ sign. While the global phase factor may not be of significant importance when compiling single-qubit gates, it manifests measurable effects in the design of two and three-qubit controlled gates. Furthermore, the phase difference between the two independent sectors of fusion charges **1** and **0** gains relevance when executing mixing operations between two qubits [37]. As a result, it is advisable to employ a global phase-independent distance metric, given that the formula in Eq. (21) precisely determines the global phases.

In the context of four Fibonacci anyons, the Hilbert space of anyon states is five dimensional. As a result of Eqs. (17), (18), and (19), the matrix representations of σ_1, σ_2, and σ_3 in the basis $\{|0\rangle,|1\rangle,|2\rangle,|3\rangle,|4\rangle\}$ given in Eqs. (5) to (9) are as follows:

$$\rho(\sigma_1) = \left(\begin{array}{cc|ccc} R^{\mathbf{0}}_{\mathbf{11}} & & & & \\ & R^{\mathbf{1}}_{\mathbf{11}} & & & \\ \hline & & R^{\mathbf{1}}_{\mathbf{11}} & & \\ & & & R^{\mathbf{0}}_{\mathbf{11}} & \\ & & & & R^{\mathbf{1}}_{\mathbf{11}} \end{array}\right), \tag{22}$$

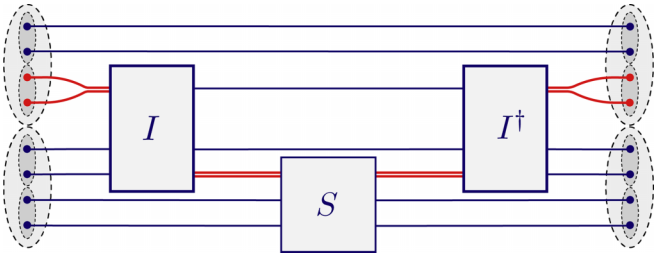

FIG. 1. In the injection method, three-strand gates can implement two-qubit gates. Notice that each lower pair of anyons in the same qubit should yield the vacuum if the state is $|0\rangle$ and yield an anyon if it is $|1\rangle$. Therefore, weaving a pair of anyons around the anyons of the controlled qubit and then returning to the initial position does not affect the state unless the state is $|1\rangle$. That is the spirit of a controlled gate.

$$\rho(\sigma_2) = \left(\begin{array}{cc|cc} (B^1_{111})^0_0 & (B^1_{111})^1_0 & & \\ (B^1_{111})^0_1 & (B^1_{111})^1_1 & & \\ \hline & & R^1_{11} & \\ & & & \begin{matrix}(B^1_{111})^0_0 & (B^1_{111})^1_0 \\ (B^1_{111})^0_1 & (B^1_{111})^1_1\end{matrix} \end{array}\right), \tag{23}$$

$$\rho(\sigma_3) = \left(\begin{array}{cc|cc} R^0_{11} & & & \\ & R^1_{11} & & \\ \hline & & (B^1_{111})^0_0 & (B^1_{111})^1_0 \\ & & R^1_{11} & \\ & & (B^1_{111})^0_1 & (B^1_{111})^1_1 \end{array}\right). \tag{24}$$

Notice that, in the sector of global charge **0**, the braid operator σ_3 has the same effect as σ_1 and the compilation of single-qubit gates in this sector is equivalent to the case of three anyons. However, the sector of global charge **1** provides a complete set of operations to process a qutrit up to a global phase determined by the winding number. Consequently, the general form will be

$$\rho(\Sigma) = \left(\begin{array}{c|c} \pm e^{-iW(\hat{B})\pi/10}[\mathrm{SU}(2)] & \\ \hline & \pm e^{iW(\hat{B})\pi/5}[\mathrm{SU}(3)] \end{array}\right). \tag{25}$$

It has been established that the weave group, which is a subgroup of the braid group, is also dense to SU(N) [38]. Weaves are defined as sequences of braids wherein a single anyon navigates around other stationary anyons. In

TABLE II. Truth table of $\mathbb{M}_4(I, S)$ gate.

Input			Output		
Qubit 1	Qubit 2	Qubit 3	Qubit 1	Qubit 2	Qubit 3
$\|0\rangle$	$\|0\rangle$	$\|\eta\rangle$	$\|0\rangle$	$\|0\rangle$	$\|\eta\rangle$
$\|0\rangle$	$\|1\rangle$	$\|\eta\rangle$	$\|0\rangle$	$\|1\rangle$	$S\|\eta\rangle$
$\|1\rangle$	$\|0\rangle$	$\|\eta\rangle$	$\|1\rangle$	$\|0\rangle$	$S\|\eta\rangle$
$\|1\rangle$	$\|1\rangle$	$\|\eta\rangle$	$\|1\rangle$	$\|1\rangle$	$\|\eta\rangle$

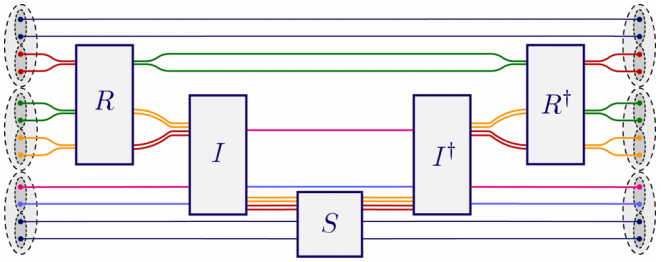

FIG. 2. General scheme of the proposed three-qubit gate by the controlled-injection method. The two upper qubits are the controlling qubits, while the lower qubit is the controlled qubit. The R operation prepares the controlling qubits while the S operation is the target operation, which is applied whenever the injected four anyons have a nontrivial overall topological charge.

diagrammatic terms, there exists a solitary warp strand that weaves around the remaining weft strands. The primary objective of this method is to simplify the implementation of braiding circuits. In scenarios involving three anyons, weaving sequences are restricted to braiding operations with even powers.

In scholarly discourse, numerous algorithms have been proposed to identify the most accurate braid sequence of a certain length that approximates a targeted unitary gate. The Solovay-Kitaev algorithm is a seminal method in this context, as it demonstrates that an approximation of a given quantum gate with a braid sequence up to the desired level of accuracy can be achieved efficiently in polylogarithmic time [37]. As per the Solovay-Kitaev theorem, the relationship between the error ϵ and the braiding length L is as follows:

$$L = \mathrm{poly}[\log(1/\epsilon)]. \tag{26}$$

Here, ϵ is proportional to any properly defined distance metric between the braid unitary matrix and the target unitary matrix in the space of unitary matrices. In this study, we utilize the

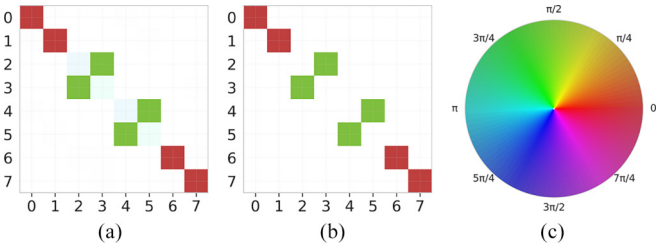

FIG. 3. (a) Matrix representation of the approximated $\mathbb{M}_4(I, iX)$ in the computational basis. The full braid matrix is 89×89 in the sector of charge **0**, while the sector **1** is irrelevant because the overall charge cannot be **1**. (b) Exact $\mathbb{M}_4(I, iX)$ matrix representation. (c) Color representation of complex numbers where the argument is ϕ and the modulus r is less than or equal to 1. The arguments are linearly transformed into the RGB color spectrum, while the modulus is converted into brightness. The brightness decreases in proportion to $e^{-r/\sigma}$, starting from 1 (white) at the center and reaching 0.5 (fully saturated) at the boundary. In this case, $\sigma = 0.01$ represents the average radius.

TABLE III. Braid sequence and accuracy of the necessary three-strand gates to approximate the $\mathbb{M}_4(I, iX)$ gate with an overall error of 6.64×10^{-4} and leakage $\epsilon_L = 3.26 \times 10^{-6}$.

$\mathbb{M}_4(R, S)$ gates	$\mathbb{M}_4(I, iX)$ gates	Weave sequence	Length	Error
R	I	$\sigma_1^{-3}\sigma_2^2\sigma_1^4\sigma_2^{-2}\sigma_1^{-4}\sigma_2^{-2}\sigma_1^2\sigma_2^2\sigma_1^4\sigma_2^4\sigma_1^2\sigma_2^{-4}\sigma_1^{-2}\sigma_2^2\sigma_1^{-2}\sigma_2^{-2}\sigma_1^2\sigma_2^{-3}$	48	1.51×10^{-3}
I	I	$\sigma_1^3\sigma_2^2\sigma_1^4\sigma_2^4\sigma_1^4\sigma_2^2\sigma_1^4\sigma_2^2\sigma_1^2\sigma_2^{-2}\sigma_1^2\sigma_2^{-2}\sigma_1^2\sigma_2^2\sigma_1^2\sigma_2^{-2}\sigma_1^2\sigma_2^{-2}\sigma_1^2\sigma_2^{-1}$	48	1.51×10^{-3}
S	iX	$\sigma_2^5\sigma_1^{-2}\sigma_2^{-2}\sigma_1^{-2}\sigma_2^{-4}\sigma_1^{-2}\sigma_2^2\sigma_1^2\sigma_2^{-4}\sigma_1^2\sigma_2^4\sigma_1^{-2}\sigma_2^4\sigma_1^{-2}\sigma_2^{-4}\sigma_1^{-2}\sigma_2^{-3}$	48	8.55×10^{-4}

spectral distance metric [26,39] to quantify the error ϵ:

$$\mathcal{D}(U_1, U_2) = \sqrt{\text{max eigenvalue}(AA^\dagger)}, \tag{27}$$

such that A is the difference between U_1 and U_2 after eliminating the global phases.

Despite the fact that the brute-force algorithm imposes an exponential demand on computational resources, it yields an optimal fundamental approximation. This suffices to provide a proof of concept for the gates introduced in subsequent sections. To render the brute-force algorithm more practical, its performance has been augmented with a number of optimizations. First, for the optimization of linear calculations, it is advantageous to map the SU(2) components of the elementary braid matrices (21) to quaternions. This approach is computationally more efficient as it reduces the number of parameters and necessitates fewer real number multiplications. Secondly, the cyclicity of the braid matrix powers should be taken into account. Specifically, $\sigma_1^{10} = \sigma_2^{10} = I$. As a result, in the context of weaves, it is adequate to span only sequences of the form σ_i^p, where $i = 1, 2$ and $p = 2, 4, 6, 8$. Thirdly, the braid group enforces algebraic relations that can effectively reduce the number of iterations over the search space. This is achieved by leveraging the similarity relation that associates each braid sequence with its counterpart, wherein σ_1 and σ_2 are permuted. Namely,

$$\sigma_1^{p_n}\sigma_2^{q_n}\cdots\sigma_1^{p_1}\sigma_2^{q_1} = \Gamma^\dagger\sigma_2^{p_n}\sigma_1^{q_n}\cdots\sigma_2^{p_1}\sigma_1^{q_1}\Gamma, \tag{28}$$

where p_i and q_i are integers and $\Gamma = \sigma_1\sigma_2\sigma_1$. The physical interpretation of the similarity relation, along with its proof and generalization, are elaborated in Appendix A. Furthermore, we illustrate in Appendix B that if the target gate is Hermitian, it suffices to span merely half of the search space. In essence, a Hermitian target gate H introduces a symmetry in the metric space since for each matrix U

$$\mathcal{D}(U, H) = \mathcal{D}(U^\dagger, H). \tag{29}$$

From a computational perspective, the utilization of a high-performance programing language can lead to substantial savings in terms of computational time, energy, memory, and development duration [40]. Furthermore, a linear acceleration is achievable by partitioning the search space across available processing units. Collectively, all algebraic and numerical optimizations significantly reduced the search time.

IV. COMPILING TOPOLOGICAL CONDITIONAL TWO-QUBIT GATES USING CONTROLLED-INJECTION METHOD

Since universality necessitates at least one entangling gate, it is imperative to devise an efficient method for constructing a two-qubit entangling gate. Employing three anyons per qubit yields five braid generators that act as $\text{SU}(5) \oplus \text{SU}(8)$ matrices, whereas employing four anyons per qubit necessitates seven braid generators in the form of $\text{SU}(13) \oplus \text{SU}(21)$ unitary matrices. Due to the vast dimensionality of the Hilbert space, the emergence of non-computational states that begin to mix with the computational space, and the substantial number of braid generators leading to an exponentially large search space, utilizing brute-force algorithms and the Solvay-Kitaev procedure may not be the most practical approach to constructing a controlled two-qubit gate [37]. Indeed, it has been found that there are systematic methods for generating controlled two-qubit gates [26,27,37]. In this section, we will review the injection method introduced in Refs. [26,37] and we will extend it to controlled three-qubit gates in the subsequent section.

The first main concept underlying the injection method that we must keep in mind is the existence of an anyonic charge that encodes the qubit. For instance, in the case of three anyons, the basis states $|0\rangle$ and $|1\rangle$ in Eqs. (2) and (3) respectively form the qubit state, with the charge of the first pair encoding the qubit state. For $|0\rangle$, the first pair has the charge $\mathbf{0}$ and, for $|1\rangle$, the first pair has the charge $\mathbf{1}$. Hence there is an inclination to weave this charge to perform specific gates. In the scenario of four anyons per qubit, the states $|0\rangle = |\mathbf{0}, \mathbf{1}, \mathbf{0}\rangle$ and $|1\rangle = |\mathbf{1}, \mathbf{1}, \mathbf{0}\rangle$ form a qubit. However, we observe that

$$|\mathbf{0}, \mathbf{1}, \mathbf{0}\rangle = |((\mathbf{1}, \mathbf{1})_{\mathbf{0}}, (\mathbf{1}, \mathbf{1})_{\mathbf{0}})_{\mathbf{0}}\rangle, \tag{30}$$

$$|\mathbf{1}, \mathbf{1}, \mathbf{0}\rangle = |((\mathbf{1}, \mathbf{1})_{\mathbf{1}}, (\mathbf{1}, \mathbf{1})_{\mathbf{1}})_{\mathbf{0}}\rangle. \tag{31}$$

Therefore, the two pairs of anyons have the same charge, which is $\mathbf{0}$ when the state is $|0\rangle$ and $\mathbf{1}$ when the state is $|1\rangle$. The second key idea is the ability to approximate the identity gate by weaving a single anyon using three anyons, with any desired level of accuracy. Consequently, the identity weave can be utilized to inject the desired controlling anyon into a specific controlled qubit and implement any targeted single-qubit gate.

TABLE IV. Truth table of the $\mathbb{M}_4(iX, S)$ gate.

Input			Output		
Qubit 1	Qubit 2	Qubit 3	Qubit 1	Qubit 2	Qubit 3
$\|0\rangle$	$\|0\rangle$	$\|\eta\rangle$	$\|0\rangle$	$\|0\rangle$	$\|\eta\rangle$
$\|0\rangle$	$\|1\rangle$	$\|\eta\rangle$	$\|0\rangle$	$\|1\rangle$	$S\|\eta\rangle$
$\|1\rangle$	$\|0\rangle$	$\|\eta\rangle$	$\|1\rangle$	$\|0\rangle$	$S\|\eta\rangle$
$\|1\rangle$	$\|1\rangle$	$\|\eta\rangle$	$\|1\rangle$	$\|1\rangle$	$S\|\eta\rangle$

TABLE V. Braid approximation of the necessary three-strand gates to compile the $\mathbb{M}_4(iX, iX)$ gate with an overall error of 6.64×10^{-4} and leakage $\epsilon_L = 3.99 \times 10^{-6}$.

$\mathbb{M}_4(R, S)$ gates	$\mathbb{M}_4(iX, iX)$ gates	Weave sequence	Length	Error
R	iX	$\sigma_1^{-1}\sigma_2^2\sigma_1^{-4}\sigma_2^2\sigma_1^{-2}\sigma_2^2\sigma_1^{-2}\sigma_2^4\sigma_1^{-2}\sigma_2^{-2}\sigma_1^{-2}\sigma_2^4\sigma_1^{-2}\sigma_2^{-2}\sigma_1^2\sigma_2^2\sigma_1^{-2}\sigma_2^{-2}\sigma_1^{-2}\sigma_2^{-2}\sigma_1^{-2}\sigma_2^1$	48	8.55×10^{-4}
I	I	$\sigma_1^3\sigma_2^2\sigma_1^4\sigma_2^4\sigma_1^4\sigma_2^2\sigma_1^4\sigma_2^2\sigma_1^2\sigma_2^{-2}\sigma_1^2\sigma_2^{-2}\sigma_1^2\sigma_2^2\sigma_1^2\sigma_2^{-2}\sigma_1^2\sigma_2^{-2}\sigma_1^2\sigma_2^{-1}$	48	1.51×10^{-3}
S	iX	$\sigma_2^5\sigma_1^{-2}\sigma_2^{-2}\sigma_1^{-2}\sigma_2^{-4}\sigma_1^{-2}\sigma_2^2\sigma_1^2\sigma_2^{-4}\sigma_1^2\sigma_2^4\sigma_1^{-2}\sigma_2^4\sigma_1^{-2}\sigma_2^{-4}\sigma_1^{-2}\sigma_2^{-3}$	48	8.55×10^{-4}

For further insights into implementing controlled two-qubit gates using three Fibonacci anyons per qubit, it is worthwhile to refer to Refs. [26,37]. In this section, we give the essence of the injection method using four anyons per qubit, which suffices for our purposes. The general structure of the gate is depicted in Fig. 1. Here, the injection gate I is employed to inject one encoding pair of anyons from the controlling qubit (the upper one) into the controlled qubit. If the controlling qubit is in the state $|0\rangle$, or equivalently the encoding pair has a trivial charge, the entire circuit is trivial and all the sequence is equivalent to the identity. However, when the injected pair has the charge **1**, the pair will, asymptotically, after the injection, assume the role of the replaced anyon in the controlled qubit. Consequently, it becomes possible to approximate the targeted gate S to any desired accuracy before reinjecting the pair back to its original position using the adjoint weave, thus avoiding any global phase residues.

V. COMPILING TOPOLOGICAL CONDITIONAL THREE-QUBIT GATES USING CONTROLLED-INJECTION METHOD

We introduce a class of quantum three-qubit gates $\mathbb{M}_n(R, S)$ that perform controlled logic operations inherently compatible with the structure of the Fibonacci model using n anyons per qubit where $n = 3, 4$. We call this method the *controlled-injection* method. We start with the case of four anyons per qubit since it is simpler to understand for this method and is the simplest encoding whose topological charge **0** sector has two dimensions. The topological sector of charge **0** for $n = 4$ serves the purpose of the exact implementation of the SWAP gate since the braiding of two **0** charges is trivial. The latter is frequently needed to implement controlled gates between nonadjacent qubits. As shown in Fig. 2, the general form of this class of three-qubit gates encodes qubits in four anyon groups. In addition, the introduced $\mathbb{M}_4(R, S)$ three-qubit gate involves three-anyon gates labeled R, I, and S, which act as $\mathrm{SU}(2) \oplus \mathrm{U}(1)$ operations, where the SU(2) part acts on the topological charge **1** sector while the U(1) part acts on the topological sector of charge **0** as shown in Eq. (21). We compile these three-anyon gates by weaving only one input anyon as explained in Sec. III. However, we are allowed to weave pairs and groups of anyons keeping in mind only the fusion outcomes of each group. In this case, the three-anyon gates will affect only the fusion state of the fusion outcomes regardless of the constituent anyons. As shown in Fig. 2, the gate R takes pairs of anyons as inputs while weaving only the upper pair, the gate I injects the upper grouped two pairs in yellow and red colors into the lower strand, and the S gate weaves the upper grouped two pairs returning them to the same strand position. In general, the $\mathbb{M}_4(R, S)$ gate works in such a way that the R gate prepares the controlling qubits, so we call it the *initialization gate*, while the S gate is the target operation to be applied on the controlled qubit; then, we call it the *target gate*. We call the intermediary identity gate the *injection gate*. To understand precisely the mechanism of this gate, we will introduce two variations of the controlled-injection three-qubit gates: $\mathbb{M}_4(I, S)$ and $\mathbb{M}_4(\mathrm{NOT}, S)$, whose initialization gates are the identity and the NOT gate, respectively.

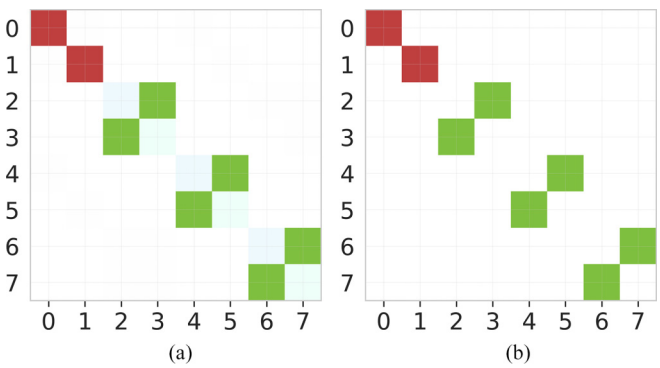

FIG. 4. (a) Matrix representation of the approximated $\mathbb{M}_4(iX, iX)$ as expressed in the basis of the computational states. (b) Exact $\mathbb{M}_4(iX, iX)$ matrix representation. The color map is depicted in Fig. 3(c).

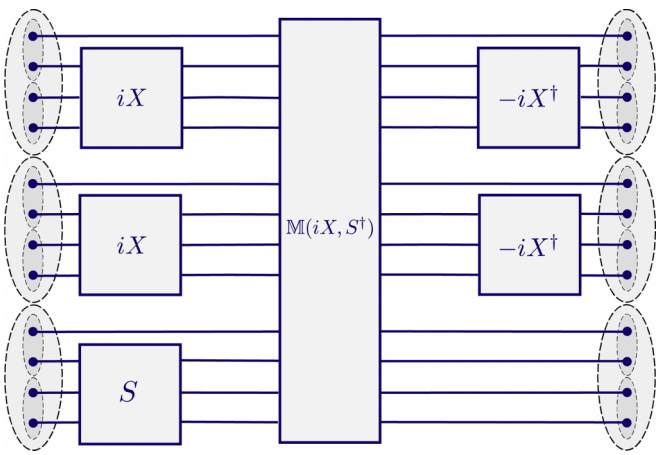

FIG. 5. To compile the CCS gate with fewer braids, it is sufficient to add NOT gates, replaced by iX and its Hermitian conjugate, and S gate to the previously defined $\mathbb{M}_4(iX, S^\dagger)$ three-qubit gate.

TABLE VI. Truth table of the CCS gate.

Input			Output		
Qubit 1	Qubit 2	Qubit 3	Qubit 1	Qubit 2	Qubit 3
$\|0\rangle$	$\|0\rangle$	$\|\eta\rangle$	$\|0\rangle$	$\|0\rangle$	$\|\eta\rangle$
$\|0\rangle$	$\|1\rangle$	$\|\eta\rangle$	$\|0\rangle$	$\|1\rangle$	$\|\eta\rangle$
$\|1\rangle$	$\|0\rangle$	$\|\eta\rangle$	$\|1\rangle$	$\|0\rangle$	$\|\eta\rangle$
$\|1\rangle$	$\|1\rangle$	$\|\eta\rangle$	$\|1\rangle$	$\|1\rangle$	$S\|\eta\rangle$

A. $\mathbb{M}_4(I, S)$ controlled-injection gate

Let us consider the initialization gate to be the identity operation, i.e., $R = I$. Notice that in the case of a four anyons qubit of overall topological charge **0**, the two constituent anyon pairs fuse simultaneously to **0** if the state is $|0\rangle$:

$$|0\rangle = |((\mathbf{1}, \mathbf{1})_{\mathbf{0}}, (\mathbf{1}, \mathbf{1})_{\mathbf{0}})_{\mathbf{0}}\rangle, \tag{32}$$

and fuse simultaneously to **1** if the state is $|1\rangle$:

$$|1\rangle = |((\mathbf{1}, \mathbf{1})_{\mathbf{1}}, (\mathbf{1}, \mathbf{1})_{\mathbf{1}})_{\mathbf{0}}\rangle. \tag{33}$$

Therefore, the identity initialization gate will have no effect but injecting the lower pair of anyons from the upper qubit into the middle qubit. If one and only one qubit of the two controlling qubits is in the state $|0\rangle$, the middle two pairs will have different topological charges with overall topological charge **1**. In contrast, when the controlling qubits are both in the state $|0\rangle$ or both in the state $|1\rangle$, the middle two pairs will have the same topological charges, and since the initialization gate approximates the identity in $\mathbb{M}_4(I, S)$, the overall topological charge of the middle two pairs will remain **0**. We summarize the truth table of this gate in Table II, where the target gate S is applied if the controlling qubits have opposite logic states. As a result, the exact matrix representation of $\mathbb{M}_4(I, S)$ should be given by

$$\left(\begin{array}{cc|cc|cc|cc} 1 & 0 & 0 & 0 & 0 & 0 & 0 & 0 \\ 0 & 1 & 0 & 0 & 0 & 0 & 0 & 0 \\ \hline 0 & 0 & \multicolumn{2}{c|}{\multirow{2}{*}{S}} & 0 & 0 & 0 & 0 \\ 0 & 0 & & & 0 & 0 & 0 & 0 \\ \hline 0 & 0 & 0 & 0 & \multicolumn{2}{c|}{\multirow{2}{*}{S}} & 0 & 0 \\ 0 & 0 & 0 & 0 & & & 0 & 0 \\ \hline 0 & 0 & 0 & 0 & 0 & 0 & 1 & 0 \\ 0 & 0 & 0 & 0 & 0 & 0 & 0 & 1 \end{array}\right). \tag{34}$$

In conclusion, the $\mathbb{M}_4(I, S)$ gate can be represented as the application of three consecutive two-qubit controlled gates. Specifically, it can be expressed as follows:

$$\mathbb{M}_4(I, S) = (\text{CNOT} \otimes I)(I \otimes \text{CS})(\text{CNOT} \otimes I). \tag{35}$$

This representation provides a clear understanding of the operation of the $\mathbb{M}_4(I, S)$ gate in terms of standard quantum gates.

1. *Numerical simulation of* $\mathbb{M}_4(I, \text{NOT})$

In practice, the initialization, injection, and target gates are approximated to a predetermined braid length. This approximation process inevitably leads to a degree of inaccuracy and leakage. To assess the efficacy of the $\mathbb{M}_4(I, \text{NOT})$ gate, we conducted a numerical simulation with the target gate chosen as the typical NOT gate, specifically $\pm iX$, the special unitary version of the NOT gate. The initial step involves identifying the weave approximation of the $\pm I$ gate for the initialization and injection gates, under the stipulation that the weft strand's initial tip takes the upper rank while its end tip takes the lower rank. Concurrently, we search for the weave approximation of the S gate, which acts on three strands, weaving the upper strand without changing its final rank. Through the optimized brute-force approach, we derived relevant weaving sequences by setting a fixed braid length of 48 braid operators and accounting for global phases. It is noteworthy that there exists a multitude of weaving sequences that exhibit optimal accuracy. In our numerical implementation, we select the weaving sequences that combine to provide the best accuracy for the $\mathbb{M}_4(I, \pm iX)$ gate. The sequences pertinent to this case are delineated in Table III.

The subsequent phase involves the conversion of these three-strand gates into a six-strand braiding circuit, as depicted in Fig. 2. Ultimately, employing the relevant matrix representations of the five elementary braid operations, a systematic numerical method developed in [36] is utilized to obtain the representation of the approximated $\mathbb{M}_4(I, iX)$ gate, as illustrated in Fig. 3. The accuracy is quantified by calculating the error using the distance metric defined in Eq. (27). The overall error of this $\mathbb{M}_4(I, iX)$ approximation is computed as 6.64×10^{-4}. The error measured solely on the controlled gate [the $S \equiv \pm iX$ block in the $\mathbb{M}_4(I, iX)$ matrix] is approximately 6.64×10^{-4}. This value is commensurate with the error computed on the $\pm iX$ approximation itself. The overall error is comparable to the error on the target because the $\mathbb{M}_4(R, S)$ is always accurate when the controlled gate is not applied since trivial braids are involved and the target gate contributes significantly to the inaccuracy.

The leakage error, denoted as ϵ_L, can also be computed. This error represents the quantity of information that the simulated gate inevitably transmits to noncomputational states. It

TABLE VII. Braid approximation of the necessary three-strand gates to build the $\pm i$Toffoli gate with overall error of 1.84×10^{-3} and leakage $\epsilon_L = 1.62 \times 10^{-6}$.

CCS gates	$\pm i$Toffoli gates	Weave sequence	Length	Error
R	iX	$\sigma_1^3\sigma_2^2\sigma_1^{-2}\sigma_2^2\sigma_1^{-2}\sigma_2^{-2}\sigma_1^{-2}\sigma_2^4\sigma_1^{-2}\sigma_2^{-2}\sigma_1^{-2}\sigma_2^2\sigma_1^{-2}\sigma_2^2\sigma_1^{-2}\sigma_2^2\sigma_1^2\sigma_2^2\sigma_1^{-2}\sigma_2^{-2}\sigma_1^2\sigma_2^{-1}$	48	8.55×10^{-4}
I	I	$\sigma_1^3\sigma_2^2\sigma_1^2\sigma_2^2\sigma_1^{-2}\sigma_2^2\sigma_1^4\sigma_2^2\sigma_1^{-2}\sigma_2^2\sigma_1^2\sigma_2^{-2}\sigma_1^4\sigma_2^4\sigma_1^2\sigma_2^{-2}\sigma_1^2\sigma_2^4\sigma_1^2\sigma_2^{-1}$	48	1.51×10^{-3}
S	iX	$\sigma_2^5\sigma_1^{-2}\sigma_2^{-2}\sigma_1^{-2}\sigma_2^{-4}\sigma_1^{-2}\sigma_2^2\sigma_1^2\sigma_2^{-4}\sigma_1^2\sigma_2^4\sigma_1^{-2}\sigma_2^4\sigma_1^{-2}\sigma_2^{-4}\sigma_1^{-2}\sigma_2^{-3}$	48	8.55×10^{-4}
NOT	iX	$\sigma_2^5\sigma_1^{-2}\sigma_2^{-2}\sigma_1^{-2}\sigma_2^{-4}\sigma_1^{-2}\sigma_2^2\sigma_1^2\sigma_2^{-4}\sigma_1^2\sigma_2^4\sigma_1^{-2}\sigma_2^4\sigma_1^{-2}\sigma_2^{-4}\sigma_1^{-2}\sigma_2^{-3}$	48	8.55×10^{-4}

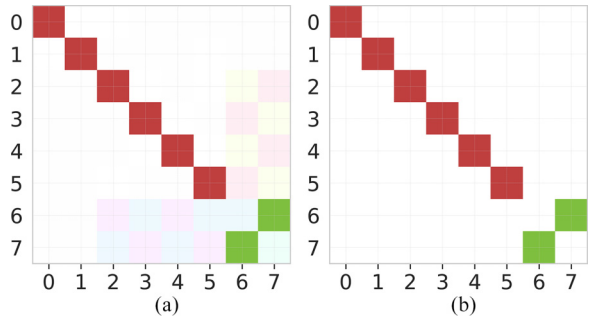

FIG. 6. (a) Matrix representation of the approximated *i*Toffoli matrix in the basis of the computational states. It represents *i*Toffoli up to 1.02×10^{-4} distance error. (c) Exact *i*Toffoli matrix representation. The color map is depicted in Fig. 3(c).

is calculated using a modified form of the spectral distance. Specifically, the leakage induced by a given gate U of d dimensions is defined as

$$\epsilon_L = 1 - \sqrt{\min \text{ eigenvalue}(UU^\dagger)}. \tag{36}$$

In this equation, the second term yields the minimum factor by which the matrix U can alter the norm of a quantum state [7]. The leakage amount measured on the simulated $\mathbb{M}_4(I, iX)$ gate is approximately 3.26×10^{-6}. It is important to note that the initialization and injection gates are anticipated to be primarily responsible for this leakage of information.

B. $\mathbb{M}_4$(NOT, S) controlled-injection gate

Let us now examine the scenario where the initialization gate assumes the role of the NOT gate, i.e., $R = \pm iX$. The complex phase $\pm i$ is essential for maintaining gates in the SU(2) group and preventing complex phases in the sector **1**, as illustrated in Eq. (21). To comprehend the effect of the initialization gate, one must revisit how the NOT gate operates on the fusion states of three Fibonacci anyons [36]. When both controlling gates are in the state $|1\rangle$, the initialization gate reverses the overall topological charge of the middle two pairs from the charge **0** to the charge **1**:

$$\text{NOT}|((\mathbf{1},\mathbf{1})_\mathbf{0},\mathbf{1})_\mathbf{1}\rangle = |((\mathbf{1},\mathbf{1})_\mathbf{1},\mathbf{1})_\mathbf{1}\rangle, \tag{37}$$

since the fusion states $|((\mathbf{1},\mathbf{1})_\mathbf{0},\mathbf{1})_\mathbf{1}\rangle$ and $|((\mathbf{1},\mathbf{1})_\mathbf{1},\mathbf{1})_\mathbf{1}\rangle$ are the only logic states in the case of three Fibonacci anyons

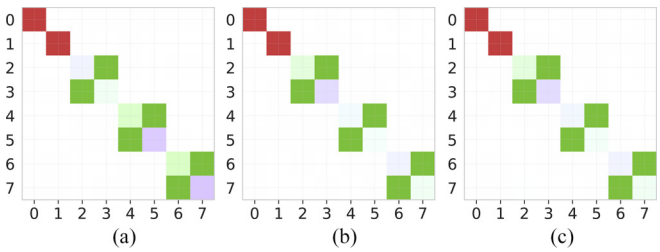

FIG. 7. Matrix representations of the approximated $\mathbb{M}_3(I, iX)$ in the computational basis considering different possible sectors: (a) sector $(\mathbf{0},\mathbf{1})$, (b) sector $(\mathbf{1},\mathbf{0})$, and (c) sector $(\mathbf{1},\mathbf{1})$. The full braid matrix is 55×55, encompassing computational and noncomputational sectors.

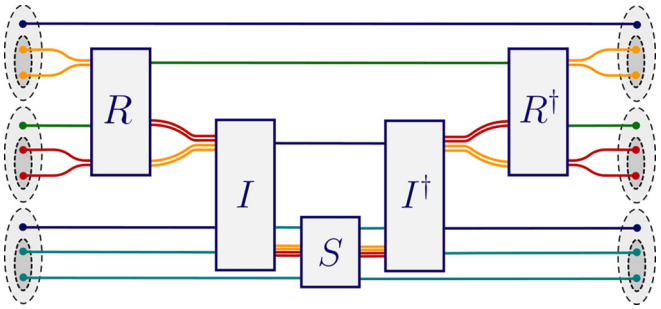

FIG. 8. This is the general scheme of the three-qubit gate by controlled-injection method using three Fibonacci anyons per qubit. The two upper qubits are the controlling qubits, while the lower qubit is the controlled qubit. R operation prepares the controlling qubits, while the S operation is the target operation implemented whenever the injected four anyons have a nontrivial overall topological charge.

in the sector of charge **1**. In other cases, the action of the initialization gate is analogous to the $R = I$ case and is trivial. Therefore, the target gate will only be operational when neither of the controlling qubits are in the $|0\rangle$ state. The truth table of $\mathbb{M}_4(iX, S)$ should align with that shown in Table IV. Consequently, the relevant matrix representation of the $\mathbb{M}_4$(NOT, S) is as follows:

$$\left(\begin{array}{cc|cc|cc|cc} 1 & 0 & 0 & 0 & 0 & 0 & 0 & 0 \\ 0 & 1 & 0 & 0 & 0 & 0 & 0 & 0 \\ \hline 0 & 0 & \multicolumn{2}{c|}{\multirow{2}{*}{S}} & 0 & 0 & 0 & 0 \\ 0 & 0 & & & 0 & 0 & 0 & 0 \\ \hline 0 & 0 & 0 & 0 & \multicolumn{2}{c|}{\multirow{2}{*}{S}} & 0 & 0 \\ 0 & 0 & 0 & 0 & & & 0 & 0 \\ \hline 0 & 0 & 0 & 0 & 0 & 0 & \multicolumn{2}{c}{\multirow{2}{*}{S}} \\ 0 & 0 & 0 & 0 & 0 & 0 & & \end{array}\right). \tag{38}$$

1. *Numerical simulation of* $\mathbb{M}_4$(NOT, NOT)

As an illustrative instance, we consider $S = \pm iX$ and set the length of the three-anyon braid gates to 48. The initial step involves identifying the compilation of $\pm iX$ and $\pm I$, ensuring that the weaving process commences from the upper strand and concludes at the lower strand. Subsequently, we seek an approximate weave for the $S = \pm iX$ gate, which operates on three strands, initiating the weaving process from the upper strand and terminating at the same strand. Utilizing an optimized brute-force approach, we derive the necessary weave sequences, as presented in Table V. These sequences are procured by spanning all combinations of the optimal individual braid sequences to enhance the accuracy of the $\mathbb{M}_4(iX, iX)$ gate.

The matrix representation of the simulated $\mathbb{M}_4(iX, iX)$ gate is depicted in Fig. 4. The computed error distance of the braid approximation is found to be 6.64×10^{-4}. However, the error of the controlled gate in the level of S blocks is approximately 6.644×10^{-4} if the controlling qubits are either in the $|01\rangle$ state or in the $|10\rangle$ state, while it is computed to be 6.637×10^{-4} if the controlling qubits are in the $|11\rangle$ state. The amount of leakage is around 3.99×10^{-6}.

C. Controlled-controlled-*S* gate with controlled-injection method

A direct application of the topological gates previously introduced is the construction of the controlled-controlled-S (CCS) gate for any unitary S up to the global phase determined by Eq. (21). The operationality of the target gate S of this controlled-controlled gate is contingent upon both controlling qubits being in the state $|1\rangle$. The implementation of the CCS gate implies the execution of the Deutsch gates $\mathbb{D}(\theta)$, which are intrinsically universal [41]. The Deutsch gate is characterized by its target gate S, defined as

$$S(\theta) = \begin{pmatrix} \cos\theta & -i\,\sin\theta \\ -i\,\sin\theta & \cos\theta \end{pmatrix} \tag{39}$$

for any angle θ. A notable gate within this class is the Toffoli gate, renowned for its ability to compute any arbitrary Boolean function, thereby qualifying it as a universal reversible logic gate [42].

One way to compile the CCS gate is to combine $\mathbb{M}_4(I, S^\dagger)$ and $\mathbb{M}_4(iX, S)$ since

$$\text{CCS} = \mathbb{M}_4(I, S^\dagger)\mathbb{M}_4(iX, S) \tag{40}$$

$$= \mathbb{M}_4(iX, S)\mathbb{M}_4(I, S^\dagger). \tag{41}$$

However, it is possible to construct a CCS gate with a single implementation of the $\mathbb{M}_4(R, S)$ gate. Initially, it should be noted that if we apply the S gate on the target qubit prior to applying the $\mathbb{M}_4(iX, S^\dagger)$ gate, we should obtain a controlled-controlled gate which operates exclusively when both of the controlling qubits are in the $|0\rangle$ state. Consequently, to produce the desired CCS gate, NOT gates should be applied on the controlling qubits both before and after the $\mathbb{M}_4(iX, S)$ is applied. Given that such NOT gates occur symmetrically, we can set them to be $\pm iX$ then $\mp iX$, specifically, to eliminate the additional phase factor on the controlling qubits. The illustration of the CCS braid circuit is depicted in Fig. 5. The corresponding truth table is detailed in Table VI. Therefore, the resulting matrix representation should be as follows:

$$\left(\begin{array}{cc|cc|cc|cc} 1 & 0 & 0 & 0 & 0 & 0 & 0 & 0 \\ 0 & 1 & 0 & 0 & 0 & 0 & 0 & 0 \\ \hline 0 & 0 & 1 & 0 & 0 & 0 & 0 & 0 \\ 0 & 0 & 0 & 1 & 0 & 0 & 0 & 0 \\ \hline 0 & 0 & 0 & 0 & 1 & 0 & 0 & 0 \\ 0 & 0 & 0 & 0 & 0 & 1 & 0 & 0 \\ \hline 0 & 0 & 0 & 0 & 0 & 0 & \multicolumn{2}{c}{\multirow{2}{*}{S}} \\ 0 & 0 & 0 & 0 & 0 & 0 & \multicolumn{2}{c}{} \end{array}\right). \tag{42}$$

1. Numerical simulation of the controlled-controlled $\pm iX$ gate

To obtain a special unitary version of the Toffoli gate, let us consider $S = \pm iX$. Initially, we should identify the compilation of $\pm I$ and $\pm iX$ such that the weaving process commences from the upper strand and concludes at the lower strand. We should also find the target $S = \pm iX$ gate acting on three strands, initiating the weaving process from the upper strand and terminating at the same strand. By employing a brute-force approach, we derived the weaving sequences, as explicitly presented in Table VII. It is important to note that these sequences are not the only possible optimal sequences. However, their combination yields the most accurate $\pm i$Toffoli gate.

Subsequently, the three-strand gates should be translated into a six-strand braiding circuit, as depicted in Fig. 2. The relevant braid matrices are then calculated, following the method employed in previous sections. Ultimately, we obtain the representation of the approximated $\mathbb{M}_4(I, iX)$ gate, as illustrated in Fig. 6. The overall distance of the approximated iToffoli gate is approximately 1.84×10^{-3}. However, the error solely on the controlled gate is about 8.55×10^{-4}. Lastly, the amount of leakage reaches 1.62×10^{-6}.

TABLE VIII. All possible fusion sectors of nine Fibonacci anyons grouped into three sets (qubits), comprising 55 fusion states distributed among four different sectors.

Independent subspaces	Sector j_1	Sector j_2	Number of states	Computational
Subspace **0**	**0**	**0**	5	No
	1	**0**	16	Yes
Subspace **1**	**0**	**1**	10	Yes
	1	**1**	24	Yes

D. Controlled injection method using three anyons per qubit

The controlled injection method is based on the manipulation of the pair of anyons responsible for encoding. In the case of three anyons, we derive the encoding basis as shown in Eqs. (4), (2), and (3). Within the charge sector **1**, the charge of the first pair encodes the qubit state. Remarkably, it is possible to replicate the $\mathbb{M}_4(\text{NOT}, S)$ gate, as depicted in Fig. 4, from the $\mathbb{M}_3(R, S)$ gate using three anyons per qubit such that $R = I$. The controlled injection method using three anyons is illustrated in Fig. 8. Additionally, it is observed that $R = \text{NOT}$ fails when both controlling qubits are in the $|1\rangle$ state. In this scenario, the noncomputational state becomes in superposition with the computational states, causing the NOT weave to act as the identity on the noncomputational state since it is single. Nevertheless, the case $R = I$ is sufficient for constructing the iToffoli gate and other controlled three-qubit gates.

Generally, when we have a group of nine anyons grouped in three sets, we can represent the fusion process state of them as follows:

$$|(((i_{11}, i_{12}), (i_{21}, i_{22}))_{j_1}, (i_{31}, i_{32}))_{j_2}\rangle, \tag{43}$$

such that $(i_{q_1}, i_{q_2}) = ((\mathbf{1}, \mathbf{1})_{iq_1}, \mathbf{1})_{i_{q_2}}$ is the fusion tree of the qth set or qubit. Consequently, the structure of the fusion space is branched into different sectors as shown in Table VIII. However, only the sectors that allow $i_{q_2} = \mathbf{1}$ for all $q = 1, 2, 3$ are computational. In conclusion, we have three computational sectors that are possible.

1. Numerical simulation of $\mathbb{M}_3(I, iX)$

First, we approximate the necessary weaves and select the best combinations that yield better overall accuracy. The approximated weaves are listed in Table IX. As a result, the evolution matrices in the computational sectors are depicted

TABLE IX. Braid sequence and accuracy of the necessary three-strand gates to approximate the $\mathbb{M}_3(I, iX)$ gate with an overall error of 1.43×10^{-3}, 2.50×10^{-3}, and 1.43×10^{-3} and leakage $\epsilon_L = 1.71 \times 10^{-6}$, 1.39×10^{-6}, and 2.57×10^{-6} in the sectors $(\mathbf{1}, \mathbf{0})$, $(\mathbf{0}, \mathbf{1})$, and $(\mathbf{1}, \mathbf{1})$, respectively.

$\mathbb{M}_3(R, S)$ gates	$\mathbb{M}_3(I, iX)$ gates	Weave sequence	Length	Error
R	I	$\sigma_1^3\sigma_2^2\sigma_1^2\sigma_2^2\sigma_1^{-2}\sigma_2^2\sigma_1^4\sigma_2^2\sigma_1^{-2}\sigma_2^2\sigma_1^2\sigma_2^{-2}\sigma_1^4\sigma_2^4\sigma_1^2\sigma_2^{-2}\sigma_1^2\sigma_2^4\sigma_1^2\sigma_2^{-1}$	48	1.51×10^{-3}
I	I	$\sigma_1^{-1}\sigma_2^2\sigma_1^4\sigma_2^2\sigma_1^{-2}\sigma_2^2\sigma_1^4\sigma_2^4\sigma_1^{-2}\sigma_2^2\sigma_1^2\sigma_2^{-2}\sigma_1^2\sigma_2^4\sigma_1^2\sigma_2^{-2}\sigma_1^2\sigma_2^2\sigma_1^2\sigma_2^3$	48	1.51×10^{-3}
S	iX	$\sigma_1^{-2}\sigma_2^{-2}\sigma_1^2\sigma_2^{-2}\sigma_1^{-2}\sigma_2^{-2}\sigma_1^4\sigma_2^{-2}\sigma_1^{-2}\sigma_2^{-2}\sigma_1^2\sigma_2^{-2}\sigma_1^2\sigma_2^{-2}\sigma_1^2\sigma_2^2\sigma_1^2\sigma_2^{-2}\sigma_1^{-2}\sigma_2^2\sigma_1^{-2}\sigma_2^{-2}$	48	8.55×10^{-4}

in Fig. 7. With this method, we are able to achieve errors of approximately 1.43×10^{-3} in the sectors $(\mathbf{1}, \mathbf{0})$ and $(\mathbf{1}, \mathbf{1})$ and 2.50×10^{-3} in the sector $(\mathbf{1}, \mathbf{1})$. These values are relatively larger in order of magnitude compared to the error obtained from the approximated $\mathbb{M}_4(iX, iX)$ as shown in Fig. 4. However, there is a tradeoff between this accuracy and the reduction in braiding cost, as will be explained later. More details about accuracies in the controlled gate are shown in Table X, which are in agreement with the visualization in Fig. 7. Finally, we observe that the amount of leakage takes the values 1.71×10^{-6} and 2.57×10^{-6}, which are slightly better than the leakage estimated for $\mathbb{M}_4(iX, iX)$ previously.

E. Comparison between controlled three-qubit gates of three and four allocations

Using three anyons per qubit for the controlled three qubit gate $\mathbb{M}_3(iX, iX)$ yields less number of braids which is in average $2(3L + 4L + 4L) = 22L$ instead of $24L$ that is required by $\mathbb{M}_4(iX, iX)$ gate, such that L is the length of R, I, and S weaves. On the other hand, $\mathbb{M}_4(iX, iX)$ gate is symmetric in implementation, i.e., we can reverse the controlling qubits easily by reversing the gate operations symmetrically relative to the horizontal line. In the case of the three anyons per qubit, it is possible to reverse controlling qubits by at least one way, which involves the application of the $F = \sigma_1\sigma_2\sigma_1$ gate (the fusion matrix), which serves as the basis transformation, to each qubit before and after the implementation of the protocol in Fig. 8.

VI. DISCUSSION

A distinctive feature of the CCS gate, compiled using the controlled-injection method, is its requirement for fewer than five two-qubit gates. Specifically, only four two-qubit gates are required: the initialization gates R and $R^\dagger$ and the injection gates I and $I^\dagger$. At first glance, this seems to contradict the theorem established in [28] which asserts that five two-qubit gates are necessary to implement the Toffoli gate. Nevertheless, it is crucial to acknowledge that this theorem relies on the Hilbert space of qubits, whereas the fusion space of anyons exhibits a distinct structure with additional dimensions. The noncomputational subspace assumes a pivotal role in the functioning of initialization gates, facilitating the formation of $\mathbb{M}_4(R, S)$ gates. In summary, the inclusion of noncomputational states makes it feasible to diminish the number of necessary two-qubit gates for the construction of a controlled three-qubit gate. Furthermore, it is instructive to examine the disparities between the controlled-injection method and the standard decomposition method of CCS gates, detailed in Appendix C. Primarily, it is worth noting that the logic tables of $\mathbb{M}_4(R, S)$ gates can additionally contribute to the diversity of quantum logic gates. Additionally, the performances of these two methods are compared in terms of four aspects: length (number of elementary braids), accuracy, leakage, and ease of implementation. A numerical comparative study of Toffoli gate compilation using both methods is depicted in Table XI. In our study, we chose the braid length to be 48 to give a reasonably acceptable approximation of the target gates up to an order of magnitude of 10^{-3}, without requiring unreasonable computational resources and long braid sequences.

Indeed, the controlled-injection method exhibits a shorter compilation length compared to the standard decomposition method. Assuming three-anyon gates of identical lengths, i.e., compiled with the same number L of braids and consuming the same amount of time to search for the best compilation, the standard decomposition method would require $6L$ braids for each controlled two-qubit gate and 16 for each SWAP gate, resulting in a total of $(30L + 32)$ braids. In contrast, the controlled-injection method requires $4L$ braids for each three-anyon gate, i.e., $20L$ braids for the $\mathbb{M}_4(iX, S)$ gate, and an additional $5L$ braids to compile the extra single-qubit gates, yielding a total of $25L$ braids. When comparing them accord-

TABLE X. Estimated accuracies and leakage amounts obtained from the simulation of the controlled-injection controlled three-qubit gate using three anyons per qubit, as illustrated in Fig. 8, with $S = i$NOT. Errors in the controlled gate are provided for the controlling qubits in the states $|01\rangle$, $|10\rangle$, and $|11\rangle$, along with overall errors and leakage amounts. Corresponding matrix representations are shown in Fig. 7.

	Errors				
	Controlled gate				
Sector	$\|01\rangle$ case	$\|10\rangle$ case	$\|11\rangle$ case	Overall	Leakage
$(\mathbf{1}, \mathbf{0})$	1.43×10^{-3}	4.97×10^{-4}	6.31×10^{-4}	1.43×10^{-3}	1.71×10^{-6}
$(\mathbf{0}, \mathbf{1})$	6.31×10^{-4}	2.24×10^{-3}	2.25×10^{-3}	2.50×10^{-3}	1.39×10^{-6}
$(\mathbf{1}, \mathbf{1})$	1.43×10^{-3}	5.70×10^{-4}	6.30×10^{-4}	1.43×10^{-3}	2.57×10^{-6}

TABLE XI. Comparative table of the controlled-injection method and the decomposition method applied on the Toffoli CCX gate as shown in Sec. V C 1 and Appendix C, respectively. The parameters considered in this comparison include the number of required three-anyon gate approximations, the total number of braids needed to compile the gate (referred to as the required braid length), and the number of sequential braids in each gate (referred to as the depth). Additionally, numerical accuracy and leakage were also evaluated. In this context, L denotes the braid length of single three-anyon gates. For the purpose of this numerical study, L was set to 48. The error statistics in the target gate and leakage values were computed over all possible combinations of the optimal weaves.

	Decomposition	Controlled injection
Two-qubit gates	7	4
Three-anyon gates	3	3
Length	$30L + 32$	$25L$
Depth	$30L + 32$	$22L$
Best error	1.90×10^{-3}	1.84×10^{-3}
Leakage of the best	3.96×10^{-6}	1.62×10^{-6}
Avg error in target	2.32×10^{-3}	2.35×10^{-3}
Min error in target	1.76×10^{-3}	8.54×10^{-4}
Max error in target	3.16×10^{-3}	3.34×10^{-3}
Avg leakage	1.75×10^{-6}	2.031×10^{-6}
Min leakage	3.93×10^{-7}	3.59×10^{-7}
Max leakage	4.09×10^{-6}	3.99×10^{-6}

ing to depth, which is the number of sequential braids, we get $(30L + 32)$ for decomposition and $22L$ for the controlled-injection method. Generally, depth is more significant in terms of compilation time. Therefore, the controlled-injection method provides gates that are at least 27% times shorter. Secondly, the controlled-injection method is as accurate as the standard decomposition method or at least within the same order of magnitude, given that the composing gates are compiled with similar accuracies. Asymptotically, both methods should exhibit behavior identical to that of the *i*Toffoli gate. This demonstrates the efficacy of the controlled-injection method in terms of accuracy, making it a viable alternative to the standard decomposition method. Thirdly, both methods were found to yield a numerically similar amount of leakage. Generally, the injection and initialization gates are the primary sources of leakage. Given that we employ injection braids of the same accuracy and leakage in both methods, a significant difference in the amount of leakage between the two methods is not anticipated. This observation underscores the comparable performance of the controlled-injection method and the standard decomposition method in terms of leakage. Lastly, the implementation of the controlled-injection method may present certain challenges, as it involves braids of multiple anyons (four anyons simultaneously), as opposed to weaving a single particle through the entire circuit. The manipulation of numerous anyons could pose significant technological hurdles [38]. Conversely, the standard decomposition can be partially transformed at the level of CNOT gates into a weaving sequence of a single particle. This transformation is feasible due to the FPF^{-1} braid circuit introduced in [37]. Thus, while the controlled-injection method offers certain advantages, its practical implementation may require overcoming additional complexities.

VII. CONCLUSION

In this study, we present an efficient topological quantum circuit model for compiling controlled-controlled gates within the Fibonacci anyon model, a versatile framework for universal quantum computing. We elevate the conventional numerical brute-force method by incorporating algebraic relations, such as similar braid sequences, and leveraging the symmetry by Hermitian target gates. Complemented by numerical methods like distributed computing, we achieve optimal approximations of single-qubit gates with three Fibonacci anyons.

In the concluding phase, we present a class of conditional three-qubit gates designed for approximating controlled logic operations, including fundamental gates like Deutsch and Toffoli. These gates are seamlessly compatible with the inherent structure of the Fibonacci model. A comparative analysis between the conventional decomposition method of three-qubit gates and the controlled-injection approach reveals that the latter allows for a more concise compilation, achieving shorter lengths and depths in implementing controlled-controlled gates, while preserving a comparable degree of accuracy and leakage.

Remarkably, the introduced controlled three-qubit gates are decomposed into four, rather than the conventional five, two-qubit gates, as stipulated by the decomposition theorem. This reduction is made possible by harnessing the noncomputational topological states within the fusion space. The controlled-injection method leverages on the unique logical attributes of the Fibonacci anyon model, presenting a potential generacy for analogous strategies across diverse anyon models or with an increased number of qubits.

ACKNOWLEDGMENTS

This document has been produced with the financial assistance of the European Union, Directorate-General for International Partnerships (Grant No. DCI-PANAF/2020/420-028) through the African Research Initiative for Scientific Excellence (ARISE), pilot program. ARISE is implemented by the African Academy of Sciences with support from the European Commission and the African Union Commission. We are grateful to the Algerian Ministry of Higher Education and Scientific Research and DGRST for the financial support.

APPENDIX A: SIMILAR BRAID SEQUENCES

The similarity relation between the braid sequences of three anyons starting with σ_1 and σ_2 has a practical use in optimizing the search for the best approximation of a given target unitary gate. The main observation that leads to similar braid sequences is the fact that applying σ_1 and σ_2 braid operations on the state $|((a, b)_i, c)_j\rangle$ of three anyons a, b, and c is equivalent to applying σ_2 and σ_1, respectively, on the state $|(c, (b, a)_i)_j\rangle$, as another observer may choose to look at the

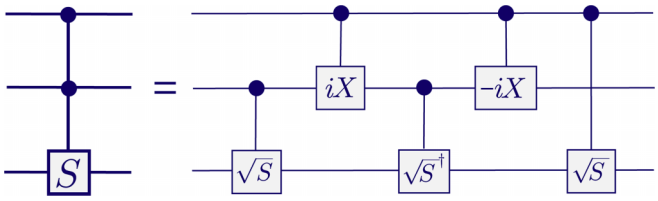

FIG. 9. Controlled-controlled-S (CCS) gate can be systematically decomposed into a sequence of five two-qubit controlled gates. This sequence comprises two controlled-NOT (CNOT) gates and two controlled gates that implement the square root of the S gate.

same set of anyons from the opposite side. In other words, σ_1 transforms to σ_2 when rotating the surface 180°. Namely,

$$|\langle((a,b)_{i'},c)_j|\sigma_1|((a,b)_i,c)_j\rangle|^2 = |\langle(c,(b,a)_{i'})_j|\sigma_2|(c,(b,a)_i)_j\rangle|^2, \tag{A1}$$

$$|\langle((a,b)_{i'},c)_j|\sigma_2|((a,b)_i,c)_j\rangle|^2 = |\langle(c,(b,a)_{i'})_j|\sigma_1|(c,(b,a)_i)_j\rangle|^2. \tag{A2}$$

This is true because, topologically, the three following operations are equivalent:

$$\sigma_1\sigma_2\sigma_1|((a,b)_i,c)_j\rangle \equiv \sigma_2\sigma_1\sigma_2|((a,b)_i,c)_j\rangle, \equiv R_{ab}R_{ic}|((a,b)_i,c)_j\rangle,$$

and

$$R_{ab}R_{ic}|((a,b)_i,c)_j\rangle = R^i_{ab}R^j_{ic}|(c,(b,a)_i)_j\rangle. \tag{A3}$$

These three operations do nothing but rotate the frame of anyons 180°. The first equivalence relation of the three is one of the Artin relations of the braid group.

Now, let us define the operator Γ such as

$$\Gamma = \sigma_1\sigma_2\sigma_1 = \sigma_2\sigma_1\sigma_2.$$

It is easy to see that

$$\sigma_1 = \Gamma^\dagger\sigma_2\Gamma, \tag{A4}$$

$$\sigma_2 = \Gamma^\dagger\sigma_1\Gamma. \tag{A5}$$

In general, a braid sequence $\mathrm{Braid}(\sigma_1,\sigma_2)$ applied on three anyons takes the form:

$$\mathrm{Braid}(\sigma_1,\sigma_2) = \sigma_1^{p_n}\sigma_2^{p_{n-1}}\cdots\sigma_1^{p_2}\sigma_2^{p_1}, \tag{A6}$$

where p_i can be any integer and $n \geqslant 2$. Therefore, the permutation between σ_1 and σ_2 yields the braid sequence $\overline{\mathrm{Braid}}(\sigma_1,\sigma_2)$ such that

$$\overline{\mathrm{Braid}}(\sigma_1,\sigma_2) = \mathrm{Braid}(\sigma_2,\sigma_1) = \sigma_2^{p_n}\sigma_1^{p_{n-1}}\cdots\sigma_2^{p_2}\sigma_1^{p_1}. \tag{A7}$$

The previous relations Eqs. (A4) and (A5) imply that Braid and $\overline{\mathrm{Braid}}$ are related by the similarity relation

$$\overline{\mathrm{Braid}}(\sigma_1,\sigma_2) = \Gamma^\dagger\mathrm{Braid}(\sigma_1,\sigma_2)\Gamma. \tag{A8}$$

This similarity relation can be deduced immediately by substitution.

1. Similarity relation for arbitrary number of anyons

To generalize the similarity relation mentioned above, we will begin by generalizing Eqs. (A4) and (A5) in Theorem 1. Subsequently, we will derive the generalized similarity relation, as expressed in Eq. (A17).

Theorem 1. For n braid generators $\sigma_1,\sigma_2,\ldots,\sigma_n$ acting on $n+1$ anyons, it holds true that

$$\sigma_i = \Gamma_n^\dagger\sigma_{n-i+1}\Gamma_n \tag{A9}$$

for $i = 1, 2, \ldots, n$, where Γ_n is defined as

$$\Gamma_n = \prod_{j=1}^{n}\prod_{k=1}^{j}\sigma_{j-k+1}. \tag{A10}$$

Here, the ordering convention of the $\prod$ operation is defined such that $\prod_{k=1}^{l}O_k = O_l\cdots O_1$. For instance, $\Gamma_2 = \prod_{j=1}^{2}\prod_{k=1}^{j}\sigma_{j-k+1} = \sigma_1\sigma_2\sigma_1$.

Proof. It suffices to use induction. First, we establish that the $n=1$ case is trivial and, for $n=2$, we obtain the Artin relation. Second, assuming the validity of the identity Eq. (A9) up to $n=m$, i.e., $\sigma_i = \Gamma_m^\dagger\sigma_{m-i+1}\Gamma_m$ for all $i = 1,\ldots,m$, we can demonstrate that for all $i = 1,\ldots,m+1$

$$\sigma_i = \Gamma_{m+1}^\dagger\sigma_{m-i+2}\Gamma_{m+1}. \tag{A11}$$

To achieve this, we should observe the recursion relation between Γ_m and Γ_{m+1}. Specifically,

$$\Gamma_{m+1} = \left(\prod_{k=1}^{m+1}\sigma_{m-k+2}\right)\Gamma_m. \tag{A12}$$

Thus, by substituting the latter and Artin relations repeatedly, we can establish Eq. (A11). Consequently, based on the validity of the first and second statements, we conclude through induction the veracity of Theorem 1. ■

For example, in the case of four anyons,

$$\sigma_1 = \Gamma_3^\dagger\sigma_3\Gamma_3, \tag{A13}$$

TABLE XII. Braid approximation of the necessary three-strand gates to build the *i*Toffoli gate with the decomposition method. We use two different best braid sequences to approximate I for controlled-NOT CNOT and C$\sqrt{\mathrm{NOT}}$ and optimize accuracy and leakage.

Gates	Target gates	Weave sequence	Length	Error
CNOT injection	I	$\sigma_1^{-3}\sigma_2^2\sigma_1^4\sigma_2^2\sigma_1^4\sigma_2^{-2}\sigma_1^2\sigma_2^{-2}\sigma_1^2\sigma_2^4\sigma_1^2\sigma_2^{-2}\sigma_1^2\sigma_2^{-4}\sigma_1^{-2}\sigma_2^{-4}\sigma_1^{-2}\sigma_2^{-3}$	48	1.51×10^{-3}
C$\sqrt{\mathrm{NOT}}$ injection	I	$\sigma_1^3\sigma_2^2\sigma_1^4\sigma_2^4\sigma_1^4\sigma_2^2\sigma_1^4\sigma_2^2\sigma_1^2\sigma_2^{-2}\sigma_1^2\sigma_2^{-2}\sigma_1^2\sigma_2^2\sigma_1^2\sigma_2^{-2}\sigma_1^2\sigma_2^{-2}\sigma_1^2\sigma_2^{-1}$	48	1.51×10^{-3}
$\sqrt{\mathrm{NOT}}$	$-i\sqrt{iX}$	$\sigma_2^{-1}\sigma_1^2\sigma_2^4\sigma_1^{-2}\sigma_2^{-4}\sigma_1^2\sigma_2^{-2}\sigma_1^2\sigma_2^4\sigma_1^{-2}\sigma_2^2\sigma_1^2\sigma_2^4\sigma_1^2\sigma_2^{-2}\sigma_1^4\sigma_2^4\sigma_1^2\sigma_2^{-1}$	48	1.24×10^{-3}
NOT	iX	$\sigma_2^5\sigma_1^{-2}\sigma_2^{-2}\sigma_1^{-2}\sigma_2^{-4}\sigma_1^{-2}\sigma_2^2\sigma_1^2\sigma_2^{-4}\sigma_1^2\sigma_2^4\sigma_1^{-2}\sigma_2^4\sigma_1^{-2}\sigma_2^{-4}\sigma_1^{-2}\sigma_2^{-3}$	48	8.55×10^{-4}

$$\sigma_2 = \Gamma_3^\dagger \sigma_2 \Gamma_3, \tag{A14}$$

$$\sigma_3 = \Gamma_3^\dagger \sigma_1 \Gamma_3. \tag{A15}$$

According to this theorem, the natural generalization of the definition of permuted braids is as follows. Given a braid sequence $\mathrm{Braid}(\sigma_1, \ldots, \sigma_n)$ applied on a number of anyons larger than or equal to n, the permuted braid is defined as

$$\overline{\mathrm{Braid}}(\sigma_1, \ldots, \sigma_n) = \mathrm{Braid}(\sigma_n, \ldots, \sigma_1). \tag{A16}$$

In conclusion, similarly to Eq. (A8), and using the same method, we can demonstrate that

$$\overline{\mathrm{Braid}}(\sigma_1, \ldots, \sigma_n) = \Gamma_n^\dagger \mathrm{Braid}(\sigma_1, \ldots, \sigma_n)\Gamma_n. \tag{A17}$$

APPENDIX B: DISTANCE SYMMETRY INDUCED BY HERMITIAN TARGET

Proposition. Let $(G, \mathcal{D})$ be a metric space such that the set G forms a group and $\mathcal{D}$ is a *bi-invariant* metric. Then, for all $a, b \in G$, if b is its own inverse (i.e., $b = b^{-1}$), it follows that $\mathcal{D}(a, b) = \mathcal{D}(a^{-1}, b)$.

A metric $\mathcal{D}$ is defined to be *bi-invariant* if, for all $a, b, c \in G$, we have $\mathcal{D}(a, b) = \mathcal{D}(ac, bc) = \mathcal{D}(ca, cb)$ [43]. Given that the set of special unitary matrices forms a group and the spectral distance Eq. (27) is bi-invariant, let H be a target unitary that is a Hermitian matrix. If $\mathcal{D}(B, H)$ is known for a given braid matrix B, then $\mathcal{D}(B^\dagger, H)$ holds the same value.

APPENDIX C: APPROXIMATED TOFFOLI GATE WITH DECOMPOSITION METHOD

The CCS gate can be decomposed to at least five two-qubit controlled operations [28,44] as shown in Fig. 9. Namely, for any unitary $\mathrm{U} \in \mathrm{U}(2)$,

$$\begin{aligned}\mathrm{CCU} = {} & (\mathrm{SWAP} \otimes I)(I \otimes \mathrm{C}\sqrt{\mathrm{U}})(\mathrm{SWAP} \otimes I) \\ & \times (\mathrm{CNOT} \otimes I)(I \otimes \mathrm{C}\sqrt{\mathrm{U}}^\dagger)(\mathrm{CNOT} \otimes I)(I \otimes \mathrm{C}\sqrt{\mathrm{U}}).\end{aligned}$$

The SWAP gate is needed because the arrangement of anyons does not allow two-qubit operation between non-neighboring three-anyons qubits without making nontrivial exchanges with the intermediary anyons. Therefore, to compile the CCS gate by decomposition, it is necessary to construct CiNOT, C$\sqrt{S}$, and SWAP gates with sufficient accuracy.

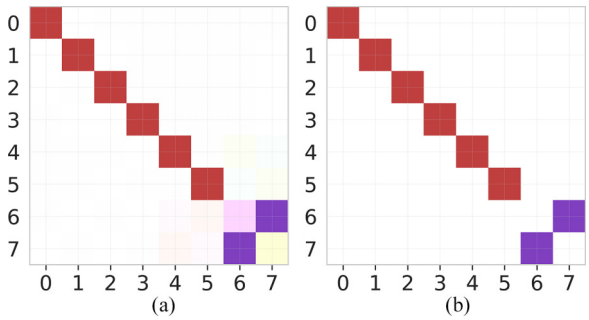

FIG. 10. (a) Matrix representation of the approximated $-i$Toffoli gate, expressed in the computational basis. (b) Exact matrix representation of the $-i$Toffoli gate. The color map is depicted in Fig. 3(c).

While the SWAP gate is trivial in the context of encoding qubits with groups of four anyons whose overall topological charge is **0**, the involved two-qubit controlled gates CiNOT and C$\sqrt{S}$ can be approximated by the injection method introduced in [26] as explained in Sec. IV and depicted in Fig. 1.

a. Numerical simulation

We should find first the compilation of $\pm I$ such that it starts weaving from the upper strand and ends up in the lower strand. We need also to approximate $\pm iX$ and $\sqrt{\pm iX}$ gates acting on three strands starting weaving from the upper strand and ending up in the same strand. By brute forcing, we find the required weaving sequences as shown in Table XII. The simulated $-i$Toffoli gate by decomposition is represented in Fig. 10. The distance error of this approximated $-i$Toffoli gate is 1.90×10^{-3}. However, the error on the controlled gate only is about 1.77×10^{-3}. The leakage is computed as well and it is 3.96×10^{-6}. These values exhibit a similar magnitude of approximation as those obtained using the controlled-injection method. However, the decomposition method generates longer braid sequences, as discussed in Sec. VI.

[1] E. Dennis, A. Kitaev, A. Landahl, and J. Preskill, J. Math. Phys. **43**, 4452 (2002).
[2] A. Kitaev, Ann. Phys. (NY) **303**, 2 (2003).
[3] M. H. Freedman, A. Kitaev, M. J. Larsen, and Z. Wang, Bull. Am. Math. Soc. **40**, 31 (2003).
[4] J. K. Pachos, *Introduction to Topological Quantum Computation* (Cambridge University Press, Cambridge, UK, 2012).
[5] V. Lahtinen and J. K. Pachos, SciPost Phys. **3**, 021 (2017).
[6] T. D. Stanescu, *Introduction to Topological Quantum Matter & Quantum Computation* (CRC Press, Boca Raton, 2017).
[7] B. Field and T. Simula, Quantum Sci. Technol. **3**, 045004 (2018).
[8] J. M. Leinaas and J. Myrheim, Nuovo Cim. B **37**, 1 (1977).
[9] F. Wilczek, Phys. Rev. Lett. **49**, 957 (1982).
[10] B. Bakalov and A. Kirillov, *Lectures on Tensor Categories and Modular Functors*, University Lecture Series (American Mathematical Society, 2000), Chaps. 1–3, pp. 1–62.
[11] E. Witten, Commun. Math. Phys. **121**, 351 (1989).
[12] J. Fröhlich, U. M. Studer, and E. Thiran, J. Stat. Phys. **86**, 821 (1997).
[13] M. H. Freedman, M. Larsen, and Z. Wang, Commun. Math. Phys. **227**, 605 (2002).
[14] M. H. Freedman, M. J. Larsen, and Z. Wang, Commun. Math. Phys. **228**, 177 (2002).
[15] T. I. Andersen, Y. D. Lensky, K. Kechedzhi, I. K. Drozdov, A. Bengtsson, S. Hong, A. Morvan, X. Mi, A. Opremcak, R. Acharya, R. Allen, M. Ansmann, F. Arute, K. Arya, A. Asfaw,

J. Atalaya, R. Babbush, D. Bacon, J. C. Bardin, G. Bortoli *et al.*, Nature (London) **618**, 264 (2023).
[16] M. Iqbal, N. Tantivasadakarn, R. Verresen, S. L. Campbell, J. M. Dreiling, C. Figgatt, J. P. Gaebler, J. Johansen, M. Mills, S. A. Moses, J. M. Pino, A. Ransford, M. Rowe, P. Siegfried, R. P. Stutz, M. Foss-Feig, A. Vishwanath, and H. Dreyer, Nature (London) **626**, 505 (2024).
[17] R. L. Willett, C. Nayak, K. Shtengel, L. N. Pfeiffer, and K. W. West, Phys. Rev. Lett. **111**, 186401 (2013).
[18] J. Nakamura, S. Liang, G. C. Gardner, and M. J. Manfra, Nat. Phys. **16**, 931 (2020).
[19] M. Aghaee, A. Akkala, Z. Alam, R. Ali, A. Alcaraz Ramirez, M. Andrzejczuk, A. E. Antipov, P. Aseev, M. Astafev, B. Bauer, J. Becker, S. Boddapati, F. Boekhout, J. Bommer, T. Bosma, L. Bourdet, S. Boutin, P. Caroff, L. Casparis, M. Cassidy *et al.*, Phys. Rev. B **107**, 245423 (2023).
[20] A. Y. Kitaev, Russian Math. Surveys **52**, 1191 (1997).
[21] M. T. Rouabah, N. E. Belaloui, and A. Tounsi, J. Phys.: Conf. Ser. **1766**, 012029 (2021).
[22] R. B. McDonald and H. G. Katzgraber, Phys. Rev. B **87**, 054414 (2013).
[23] L. Moro, M. G. A. Paris, M. Restelli, and E. Prati, Commun. Phys. **4**, 178 (2021).
[24] V. Kliuchnikov, A. Bocharov, and K. M. Svore, Phys. Rev. Lett. **112**, 140504 (2014).
[25] E. G. Johansen and T. Simula, PRX Quantum **2**, 010334 (2021).
[26] N. E. Bonesteel, L. Hormozi, G. Zikos, and S. H. Simon, Phys. Rev. Lett. **95**, 140503 (2005).
[27] C. Carnahan, D. Zeuch, and N. E. Bonesteel, Phys. Rev. A **93**, 052328 (2016).
[28] N. Yu, R. Duan, and M. Ying, Phys. Rev. A **88**, 010304(R) (2013).
[29] H. Xu and J. M. Taylor, Phys. Rev. A **84**, 012332 (2011).
[30] J. Slingerland and F. Bais, Nucl. Phys. B **612**, 229 (2001).
[31] M. A. Levin and X.-G. Wen, Phys. Rev. B **71**, 045110 (2005).
[32] N. E. Bonesteel and D. P. DiVincenzo, Phys. Rev. B **86**, 165113 (2012).
[33] P. H. Bonderson, Non-Abelian Anyons and Interferometry, Ph.D. thesis, California Institute of Technology, 2007.
[34] S. H. Simon, *Topological Quantum* (Oxford University Press, London, England, 2023).
[35] R. Ainsworth and J. K. Slingerland, New J. Phys. **13**, 065030 (2011).
[36] A. Tounsi, N. E. Belaloui, M. M. Louamri, A. Mimoun, A. Benslama, and M. T. Rouabah, arXiv:2307.01892.
[37] L. Hormozi, G. Zikos, N. E. Bonesteel, and S. H. Simon, Phys. Rev. B **75**, 165310 (2007).
[38] S. H. Simon, N. E. Bonesteel, M. H. Freedman, N. Petrovic, and L. Hormozi, Phys. Rev. Lett. **96**, 070503 (2006).
[39] S. Khatri, R. LaRose, A. Poremba, L. Cincio, A. T. Sornborger, and P. J. Coles, Quantum **3**, 140 (2019).
[40] In this study, the C++ language, recognized as one of the contemporary high-performance languages [45], is employed.
[41] D. Deutsch, Proc. R. Soc. London, Ser. A **425**, 73 (1989).
[42] T. Toffoli, in *Automata, Languages and Programming* (Springer, Berlin, 1980), pp. 632–644.
[43] D. Q. Huynh, J. Math. Imaging Vision **35**, 155 (2009).
[44] A. Barenco, C. H. Bennett, R. Cleve, D. P. DiVincenzo, N. Margolus, P. Shor, T. Sleator, J. A. Smolin, and H. Weinfurter, Phys. Rev. A **52**, 3457 (1995).
[45] R. Pereira, M. Couto, F. Ribeiro, R. Rua, J. Cunha, J. A. P. Fernandes, and J. A. Saraiva, in *Proceedings of the 10th ACM SIGPLAN International Conference on Software Language Engineering*, SLE 2017 (Association for Computing Machinery, New York, 2017), pp. 256–267.